Geoscientific
Model Development
Discussions

Coupling framework (1.0) for the ice sheet model PISM (1.1.1) and the ocean model MOM5 (5.1.0) via the ice-shelf cavity module PICO

Moritz Kreuzer[1,2], Ronja Reese[1], Willem Nicholas Huiskamp[1], Stefan Petri[1], Torsten Albrecht[1], Georg Feulner[1], and Ricarda Winkelmann[1,2]

[1]Earth System Analysis, Potsdam-Institute for Climate Impact Research (PIK), Member of the Leibniz Association, P.O. Box 60 12 03, 14412 Potsdam, Germany
[2]University of Potsdam, Institute of Physics and Astronomy, Karl-Liebknecht-Str. 24-25, 14476 Potsdam, Germany

Correspondence: Moritz Kreuzer (kreuzer@pik-potsdam.de), Ricarda Winkelmann (ricarda.winkelmann@pik-potsdam.de)

Abstract. The past and future evolution of the Antarctic Ice Sheet is largely controlled by interactions between the ocean and floating ice shelves. To investigate these interactions, coupled ocean and ice sheet model configurations are required. Previous modelling studies have mostly relied on high resolution configurations, limiting these studies to individual glaciers or regions over short time scales of decades to a few centuries. We present a framework to couple the dynamic ice sheet model PISM

5 with the global ocean general circulation model MOM5 via the ice-shelf cavity module PICO. Since ice-shelf cavities are not resolved by MOM5, but parameterized with the box model PICO, the framework allows the ice sheet and ocean model to be run at resolution of 16 km and 3°, respectively. This approach makes the coupled configuration a useful tool for the analysis of interactions between the entire Antarctic Ice Sheet and the Earth system over time spans on the order of centuries to millennia. In this study we describe the technical implementation of this coupling framework: sub-shelf melting in the

10 ice sheet model is calculated by PICO from modeled ocean temperatures and salinities at the depth of the continental shelf and, vice versa, the resulting mass and energy fluxes from the melting at the ice-ocean interface are transferred to the ocean model. Mass and energy fluxes are shown to be conserved to machine precision across the considered model domains. The implementation is computationally efficient as it introduces only minimal overhead. The framework deals with heterogeneous spatial grid geometries, varying grid resolutions and time scales between the ice and ocean model in a generic way, and can

15 thus be adopted to a wide range of model setups.

1 Introduction

Most of Antarctica's coastline is comprised of floating ice shelves where glaciers of the Antarctic Ice Sheet (AIS) drain into the surrounding Southern Ocean. Mass loss of these ice shelves is dominated by ocean-induced melting from below or calving

20 of icebergs (Depoorter et al., 2013). Observations show that ice shelf-ocean interaction has been the main driver for mass loss of the West Antarctic Ice Sheet for the past 25 years (Jenkins et al., 2018; Shepherd et al., 2018; Holland et al., 2019). As the

Geoscientific
Model Development
Discussions

ice shelves have a buttressing effect on the inland ice streams, they play a key role for the overall mass loss of the AIS (Fürst et al., 2016; Reese et al., 2017; Gudmundsson et al., 2019).

Ocean forcing also plays an important role in the paleo-climatic context (Hillenbrand et al., 2017; Lowry et al., 2019). While
25 ice-sheet simulations usually rely on external forcing without interactive coupling to calculate sub-shelf melt rates (Pollard et al., 2016; Sutter et al., 2016; Albrecht et al., 2020), general circulation models usually use prescribed ice-sheet configurations (Kageyama et al., in review, 2020). Ice-sheet models have been coupled to Earth system models of intermediate complexity (Ganopolski and Brovkin, 2017) and also to General Circulation Models (Gierz et al., 2015; Goelzer et al., 2016; Ziemen et al., 2019). These coupled setups are using, if they consider ocean forcing on the ice sheet, simple melt parameterisations that do
30 not take the circulation in ice-shelf cavities into account, which is important to estimate realistic melt rates.

Substantial progress has been made in projecting the future Antarctic sea-level contribution using standalone ice-sheet models in community-wide model intercomparison projects, including the Linear Antarctic Response Model Intercomparison Project (LARMIP-2; Levermann et al., 2014, 2020) and the Ice Sheet Model Intercomparison Project for CMIP6 (ISMIP6; Nowicki et al., in review, 2020; Seroussi et al., in review, 2020), where ice-sheet models were forced by atmospheric and
35 oceanic boundary conditions from the Coupled Model Intercomparison Project CMIP5 (Taylor et al., 2012). Similarly, CMIP5 models have been used to drive regional ocean models which allows the projection of changes in the Southern Ocean at resolutions that permit ice-shelf cavities to be resolved (Naughten et al., 2018). In particular, projected changes under high emission climate scenario A1B can possibly push the large cavity of Filchner-Ronne Ice Shelf from its current cold state to shift into a warm state, implying highly non-linear behaviour (Hellmer et al., 2017).

40 Considerable advances have been made in interactive modeling of ice-sheet/ocean interactions (Dinniman et al., 2016; Asay-Davis et al., 2017), in particular through recent intercomparison projects (Asay-Davis et al., 2016). Existing coupling approaches focus mostly on models with high spatial resolution which explicitly resolve the cavities underneath the floating ice shelves but come with the downside of heavy computational cost. Current approaches either use idealised setups (De Rydt and Gudmundsson, 2016; Favier et al., 2019) or focus on short timescales of decades to a few centuries, in which ice-ocean
45 interactions are modeled for configurations of particular regions of the AIS, as for example the Filchner-Ronne Ice Shelf in Timmermann and Goeller (2017), Thwaites Glacier in Seroussi et al. (2017) or the Amundsen Sea Sector in Donat-Magnin et al. (2017). While the detailed representation of sub-shelf processes is important for realistic estimates of melt rates, these highly-resolved configurations are not applicable to examine long-term and global effects of ice-ocean interaction.

This is crucial because including freshwater fluxes from the Antarctic Ice Sheet in simulations of Global Circulation Models
50 has been shown to influence global ocean temperatures and their variability (Golledge et al., 2019), precipitation patterns (Bronselaer et al., 2018) as well as to increase Antarctic ice loss through trapping warm water below the sea surface (Bronselaer et al., 2018; Golledge et al., 2019). Therefore, as an important next step, modeling dynamic exchange between land ice and ocean systems is required on a global and centennial to multi-millennial scale to represent relevant feedbacks and constrain potential thresholds or tipping points in the ice sheet as well as the ocean.

55 There is hence a need to bridge the gap between a physically accurate representation of the melting processes in the ice shelf cavities on the one hand, and applicability of ice-ocean interaction modelling on a global scale over glacial cycle time

Geoscientific
Model Development
Discussions

scales on the other hand. To address this, we present a framework for the dynamical coupling of the Parallel Ice Sheet Model (PISM; Bueler and Brown, 2009; Winkelmann et al., 2011) and a coarse resolution configuration of the Modular Ocean Model (MOM5; Griffies, 2012) using the Potsdam Ice-shelf Cavity mOdule (PICO; Reese et al., 2018). PICO extends the ocean

60 box model by Olbers and Hellmer (2010) for application in 3-dimensional ice sheet models. It approximates the vertical overturning circulation underneath ice shelves and includes melting physics at the ice-ocean interface, which allows the model to capture the dominant melt processes while being computationally efficient at the same time. This framework provides a tool to address scientific questions on centennial to millennial time scales or large ensemble runs to constrain parameter and model uncertainties.Yet, the presented coupling framework is not limited to a certain set of model configurations (like the coarse

65 ocean grid in use here) and generic enough to also handle high-resolution model setups.

The design of the presented framework follows three criteria: (1) mass and energy conservation needs to be ensured over both ocean and ice sheet model domains, (2) the coupling framework should not introduce a performance bottleneck to the existing standalone models and (3) the framework should follow a generic and flexible design independent of specific grid resolutions or number of deployed CPUs.

70 In the following we introduce the ice-sheet model and ocean model in use, including their grid definitions (Section 2). The framework design including the variables that are exchanged between the models is discussed in Section 3, followed by a detailed description of inter-model data processing in Section 4. The framework performance and conservation of mass and energy are evaluated in Section 5, followed by a discussion (Section 6) and conclusions (Section 7).

2   Models

75 The following paragraphs introduce the ice-sheet model PISM including its sub-shelf cavity module PICO and the ocean model MOM5 that are coupled in the framework.

2.1   Ice Sheet Model PISM and the ice-shelf cavity module PICO

The Parallel Ice Sheet Model[1] (PISM) is an open-source, three-dimensional, thermodynamically-coupled model which simulates ice sheets and ice shelves using a finite-difference discretisation (Bueler and Brown, 2009; Winkelmann et al., 2011).

80 PISM is defined on a regular Cartesian grid as shown in Fig. 1a, which is projected on a WGS84 ellipsoid (Slater and Malys, 1998) or related geometries like a perfect sphere. In this work PISM is used with a horizontal resolution of $16\mathrm{km} \times 16\mathrm{km}$ with 80 vertical levels (Albrecht et al., 2020). However, the coupling framework is generic and can handle different resolutions of the PISM grid. The numerical time-stepping scheme is adaptive and based on the Courant-Friedrichs-Lewy (CFL) condition among others (Bueler et al., 2007), which results in a range of time steps from minutes to years depending on the physical state

85 of the model. The PISM source code is written in C++.

The Potsdam Ice-shelf Cavity mOdel (PICO) calculates sub-shelf melt rates and is implemented as a submodule of PISM (Reese et al., 2018). It parameterises the vertical overturning circulation in ice-shelf cavities driven by the ice-pump mechanism,

---

[1]see https://pism-docs.org/ (last accessed: August 24, 2020)

as described by Lewis and Perkin (1986). This circulation induces melting and freezing below the ice shelves which is shown
in Fig. 3. PICO uses a box representation below the ice shelves developed by Olbers and Hellmer (2010) and extends their

90   approach to two horizontal dimensions. Input for PICO are ocean temperature and salinity at the depth of the continental
shelf. The strength of the overturning circulation is calculated in PICO from the density difference between the inflowing
water masses and the water masses in the first box close to the grounding line and scaled with a continent-wide overturning
coefficient, which is an internal PICO parameter that requires sensible tuning. Thus no ocean model velocities are required for
input to PICO.

2.2   Ocean Model MOM5

The ocean model in use for this coupling setup is the Modular Ocean Model v5[2] (MOM5; Griffies, 2012) which is an open-
source, three-dimensional Ocean General Circulation Model (OGCM) . It is coupled via the Flexible Modelling System (FMS)
coupler to the Sea Ice Simulator (SIS; Winton, 2000). In this work, we also include SIS and FMS when referring to MOM5.
For this study, MOM5 is used with a global coarse grid setup from Galbraith et al. (2011, see Fig. 1b): the lateral model grid

100   is $3°$ resolution in longitude (120 cells) and in latitude it varies from $3°$ at the poles to $0.6°$ at the equator (80 cells). The
vertical grid is defined using the re-scaled pressure coordinate (p^*) with a maximum of 28 vertical layers. The uppermost eight
layers are approximately $10\,\mathrm{m}$ thick, gradually increasing for deeper cells. The lowermost cells can have a reduced thickness
to account for ocean bathymetry with partial cells. The ocean grid is not defined in the center of the Antarctic continent (south
of $\approx 78°$S, see Fig. 1b). The ocean-sea ice system time steps are set to 8 hours. MOM5, SIS and FMS are written in Fortran.

3   Coupling Approach

The design of the coupling between the ice-sheet model PISM and the ocean model MOM5 is shown in Fig. 2, including the
exchanged variables. PICO requires two dimensional (horizontal) input fields, namely temperature and salinity of water masses
that access the ice-shelf cavities, to calculate melting and refreezing at the ice-ocean interface, as illustrated in Fig. 3. The ice
model fluxes for basal melt, surface runoff and calving are used to determine the mass as well as energy fluxes received by the

110   ocean model.

   The time scales of physical processes as well as the numerical time steps in MOM5 (hours) and PISM (years) differ by
several orders of magnitude. This is one motivation among others to use an *offline coupling* approach to exchange the fields
between the two distinct models. In this case both models are run in alternating order for the same model time, which will be
referred to as the *coupling time step*. This technical procedure is illustrated in Fig. 4. An alternative *online coupling* approach

115   is discussed in Section 6. During offline coupling, the model output after each model integration step is processed and provided
as input or boundary condition to the other model, respectively. Using the modified input, the models are restarted from their
previous computed state. For example, MOM5 runs for 10 years and writes annual mean diagnostics fields of temperature and
salinity. PISM receives the last of these averaged fields as boundary conditions for PICO, and is then integrated for the same 10

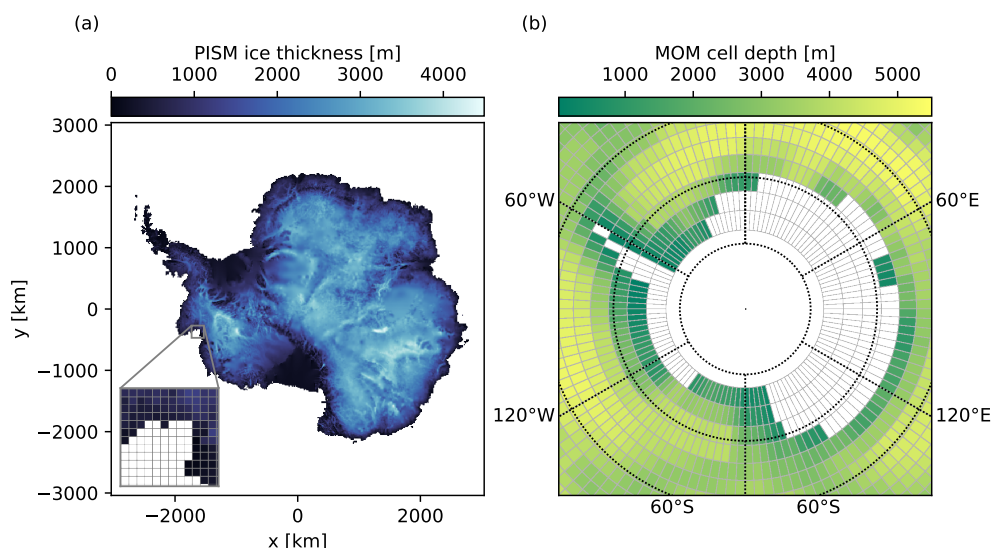[2]see https://mom-ocean.github.io/ (last accessed: August 24, 2020)

Figure 1. Ice-sheet and ocean model grids. (a) Ice thickness in Antarctica on the Cartesian PISM grid. The inset shows the grid structure in a coastal area for a resolution of 16 km. (b) Depth of MOM5 cells displayed in stereographic projection centered at the South Pole. Resolution at $70°\,$S is $\sim 3°$lat$\times 3°$lon ($\sim 330\,$km$\times 115\,$km). White cells are considered land by MOM5. The ocean grid extends to $78°$S. Interlocking of PISM and MOM5 domains is shown in Fig. 3 and 6a.

Figure 2. Overview of the coupling framework showing the input and output variables for the ocean model MOM5 and the ice-sheet model PISM. Dimensions of variables are given in parentheses, units in square brackets. The (lat,lon) coordinates refer to the spherical ocean model grid and the (x,y) coordinates to the Cartesian ice sheet model grid.
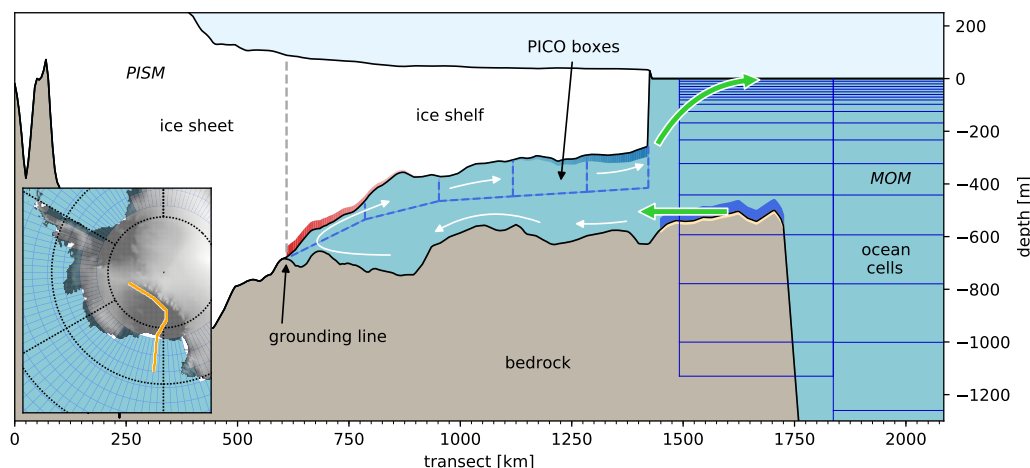
5

Figure 3. Coupling framework for the ice-sheet model PISM and the ocean model MOM5 via the ice shelf cavity module PICO. A cross section of PISM bedrock (brown) and ice thickness (white) is compared to the MOM5 ocean cells (blue continuous lines). The inset shows the transect line in orange colour in the Antarctic region. PICO boxes (blue dashed lines) follow the overturning circulation in the ice-shelf cavity. The circulation is indicated by white arrows with highest melting in the deepest regions close to the grounding line (red shade) and lower melting or refreezing in the shallower areas towards the ice shelf front (blue shade). The exchange of variables and fluxes between the two models is indicated by green arrows: PICO input from MOM5 is taken at the depth of the continental shelf (light brown region). Mass and energy fluxes from PICO are transferred to MOM5 through the surface runoff interface.

year period. Melt water and energy fluxes derived from PISM output are aggregated over the coupling time step. The resulting
120 fluxes are then added as external fluxes to the ocean over the course of the next integration period. To avoid shocks in the forcing, they are distributed uniformly over the entire coupling time step.

The coupling framework consists of a Bash script which implements the coupling procedure indicated in Fig. 4, making use of the software tools Climate Data Operator (CDO; Schulzweida, 2019) and netCDF Operator (NCO; Zender, 2018). The output processing between the different model executions is implemented in Python scripts. Their functionality will be
125 explained in the next Section. The code is made available in a public archive[3], see also the "Code and data availability" section below.

4 Inter-Model Data Processing

To make the output of the ocean model compatible with the input requirements of the ice model and vice versa, processing of data output fields like regridding, adjustment of dimensions, unit conversion or filling of missing values is required, which is
130 described in this section.

---

[3]https://doi.org/10.5281/zenodo.3998126 (last accessed: August 24, 2020)
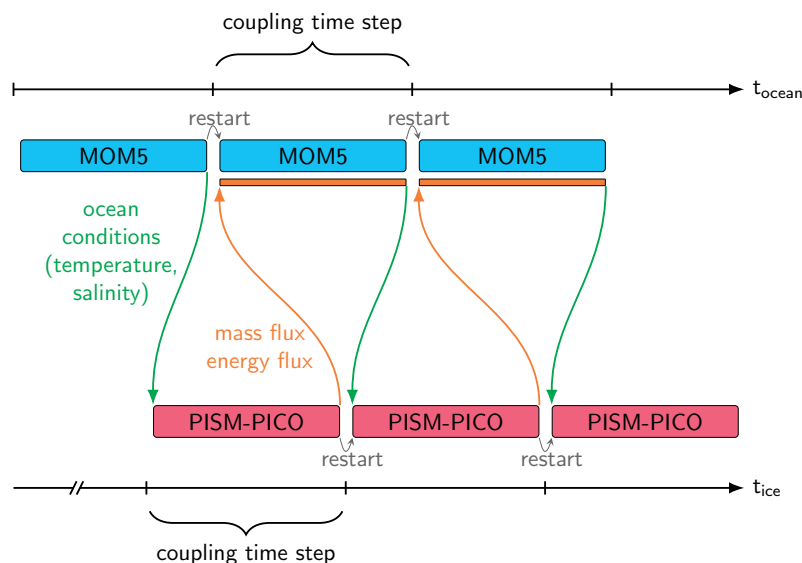
Figure 4. Offline coupling procedure for the PISM-MOM5 setup: the models are run sequentially for the same coupling time step and after each run, variables are exchanged. Sharing the same time axis is technically not compulsory but recommended. Temperature and salinity variables from the ocean model MOM5 are used as input fields for PISM-PICO. Mass and energy fluxes from PISM-PICO output are uniformly applied over the next coupling time step as input to MOM5.

The ice and ocean models operate on independent, non-complementary computational grids. The inset of Fig. 3 shows that there are both, spatial gaps and overlaps, between the ocean grid cells and the ice extent represented by PISM. As the ocean grid is much coarser than the ice grid and MOM5 cells are either defined entirely as land or ocean (no mixed cells allowed), inconsistencies in the horizontal grid entanglement are unavoidable, requiring careful consideration of data exchange. The grid

135 remapping mechanisms presented in the following sections are independent of the used grid resolutions.

4.1 Ocean to Ice

PICO uses a definition of ocean basins around the Antarctic Ice Sheet which encompass areas of similar ocean conditions at the depth of the continental shelf (Reese et al., 2018). They are based on Antarctic drainage basins defined in Zwally et al. (2012) and extended to surrounding ice sheets and the Southern Ocean, see Fig. 5b. Oceanic fields of temperature and salinity

140 are averaged over the continental shelf for each basin and provided as input to PICO. Note that PICO uses one value of temperature and salinity per basin. Three steps are needed to process the oceanic output fields to make them usable as input to PISM:

    – First, the three dimensional output fields (temperature, salinity) are remapped bilinearly from the spherical ocean grid to the Cartesian ice grid. Bilinear regridding is chosen to allow for a smooth distribution of the coarse ocean cell quantities

145   on the finer ice grid. Through regridding, regions with missing values on the ice grid increase (e.g., compare the ocean
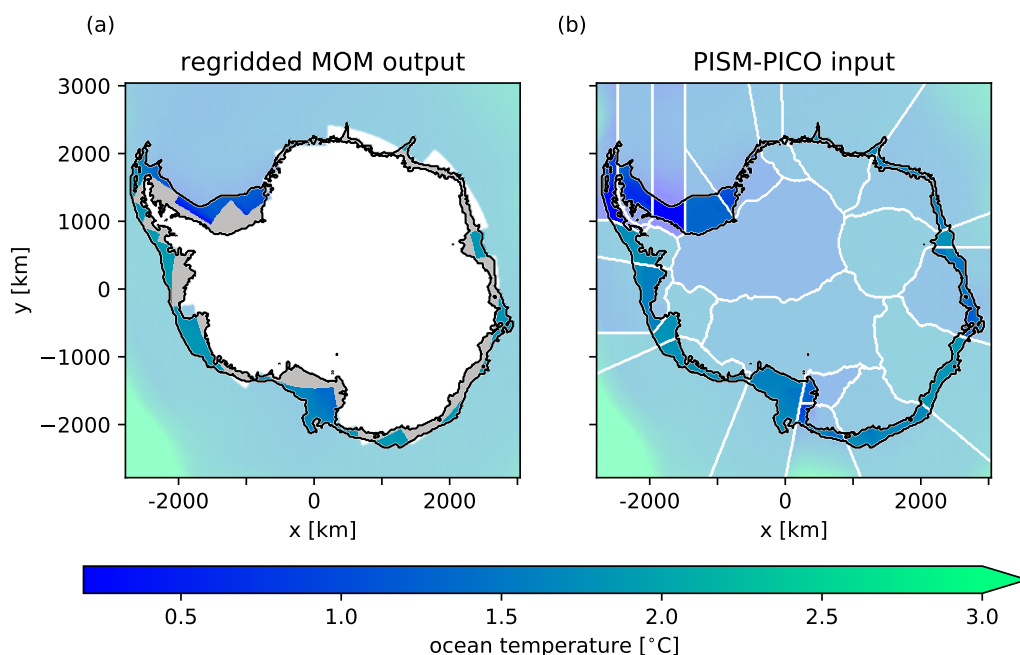
7

Figure 5. Visualisation of inter-model data processing from (a) regridded ocean model output to (b) ice model input. In (a) an example for the ocean temperature field at a depth of approximately $500\,\mathrm{m}$ is shown, with black contour lines indicating the continental shelf between the ice shelf front and the continental shelf break (-2000 m) as used in PICO. Missing values within that area are coloured in grey. Ocean values outside the continental shelf are not used for averaging basin mean values in PICO and therefore shown in lighter colours. The result of the processing procedure is the two dimensional ocean temperature field shown in (b), which is obtained through vertical interpolation of the filled fields applied to appropriate basin depths. PICO basins are indicated by white contour lines.

coverage around the Antarctic Peninsula in Fig. 1b and 5a for example). This is a consequence of bilinear regridding, which interpolates values between the cell centers of non-missing source grid cells and not the cell boundaries.

– Secondly, missing values are filled with appropriate data, namely the average over all existing values that are adjacent to grid cells with missing values. This procedure is conducted for each basin and vertical layer. Now, the continental shelf area between the ice shelf front and the continental shelf break (see Figure 5a), which is used by PICO to calculate the basin mean values of oceanic boundary conditions, is entirely filled with appropriate values.

– Lastly, the three dimensional variables are reduced to two dimensional PICO input fields which represent the ocean conditions at the depth of the continental shelf. This is done by vertical linear interpolation: for every horizontal grid point, the data is interpolated to PISM's mean continental shelf depth of the corresponding basin. An example of the processed input data for PICO is shown in Fig. 5b.
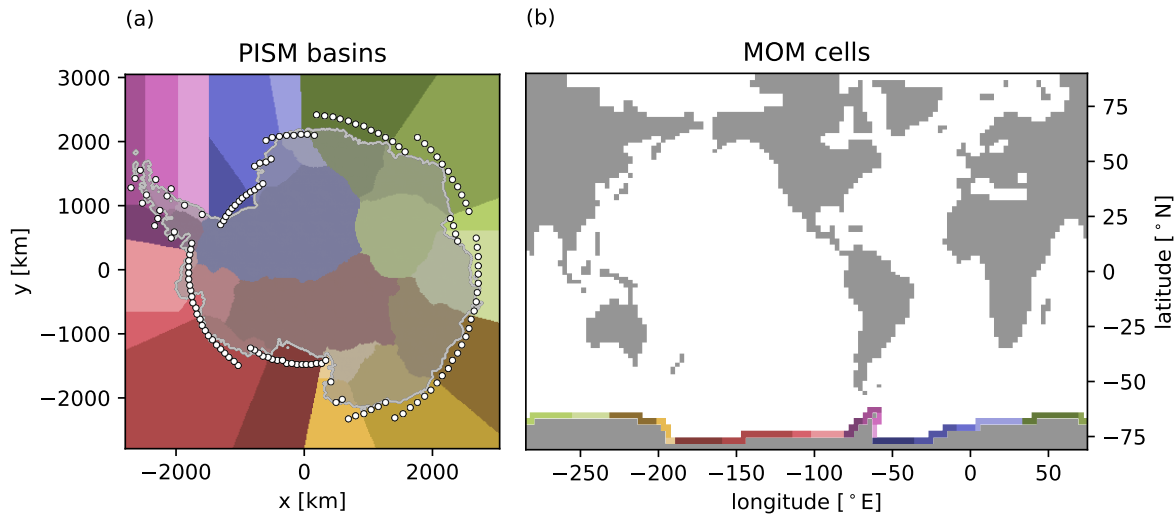
Figure 6. Visualisation of mapping mechanism between (a) PICO basins and (b) MOM5 ocean cells. PICO basins on the ice-sheet grid are shown in (a), with each basin assigned a different colour. The location of the centre of southernmost ocean cells is denoted by white circles. As a spatial reference, the ice cover modelled by PISM is shown in grey. Panel (b) shows the MOM5 land-ocean mask with corresponding PICO basin colours for the southernmost ocean cells surrounding the Antarctic Ice Sheet. Grey cells are considered as land in MOM5.

4.2 Ice to Ocean

To transfer the mass and energy fluxes from the ice model to the ocean model, a mapping from the PISM to the MOM5 grid is required. Since large areas of the PISM domain are not overlapping with valid MOM5 ocean cells (see white areas in Fig. 1b and inset in Fig. 3), common regridding algorithms would ignore quantities in those areas and consequently violate mass and
160 energy conservation.

Thus we introduce a new mechanism for the coupled system which maps every southernmost ocean cell of the MOM5 grid to exactly one PICO basin (see Fig. 6). The mechanism selects the basin that the center of the MOM5 cell lies in. In general, one basin is linked this way to multiple ocean cells and the basin share $1/n$ is stored for each ocean cell, with n being the number of ocean cells mapped to the same basin. The PISM mass and energy fluxes in each coupling time step are then aggregated per
165 basin and subsequently distributed to the related MOM5 ocean cells. An example for PISM mass fluxes and their distribution onto the MOM5 grid is shown in Fig. 7.

The mass and energy fluxes from PISM output are calculated and distributed in the following manner:

- The PISM output variables describing the surface runoff, basal mass fluxes and discharge through calving are added up. As they are given in units of $\mathrm{kg/m^2}$ and temporally aggregated, multiplication with the PISM grid cell areas and division
170 by the integration interval transforms the consolidated mass flux into units of $\mathrm{kg/s}$.
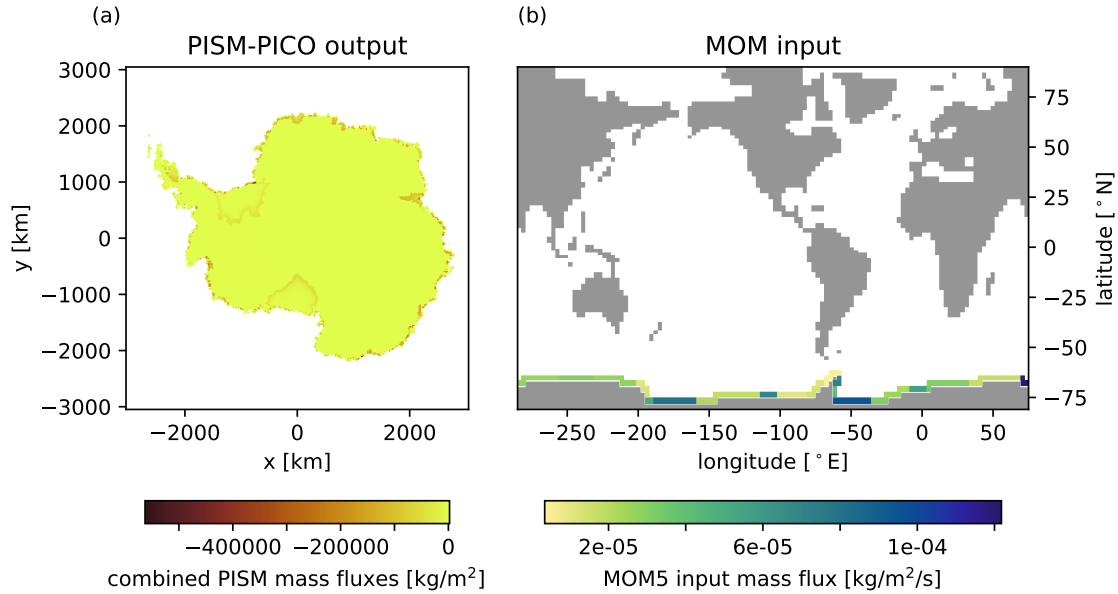
9

Figure 7. Visualisation of (a) PISM mass flux distribution to (b) the MOM5 ocean grid. PISM output variables describing surface runoff, basal melting and calving are aggregated to calculate mass and energy fluxes which are processed as input to the MOM5 ocean model as described in Section 4.2. Panel (b) shows the corresponding mass flux distribution on the MOM5 grid.

– The energy flux from ice to ocean is obtained by multiplying the mass flux resulting from basal melt and discharge with the enthalpy of fusion ($L = 3.34 \cdot 10^5 \, \text{J/kg}$) to account for the energy required during the phase change from frozen to liquid state or vice versa. At this point the energy flux is in the unit W. Potential diffusive heat fluxes from the ocean into the ice as well as the energy required to warm the melt water to ambient temperatures are comparatively small (Holland and Jenkins, 1999) and thus neglected here.

– Having calculated bulk mass and energy fluxes, they can be aggregated for each PICO basin and distributed to the corresponding ocean cells with the mapping mechanism described above. On the ocean grid the fluxes are divided by the given grid cell area resulting in unit kg/s/m^2 for mass and W/m^2 for energy fluxes. These fluxes are input into the ocean surface through MOM5's FMS coupler.

5 Results

In this section, the coupling setup will be evaluated on the basis of runtime performance and numerical accuracy. Physical evaluation of the coupled setup and implications in terms of possible feedback mechanisms will be studied in detail in a separate article.

5.1 Coupled Benchmarks

185 The coupling framework presented here provides the tools for coupled ice sheet-ocean simulations on centennial to millennial time scales, which requires reasonably fast execution times. In the following, we analyse the coupled execution time and evaluate the efficiency of the coupling framework, using a total model runtime of 200 years on 32 cores (2 CPU nodes, each equipped with 2×8 core Intel E5-2667 v3). For the modelling of ice-ocean interactions, the coupling time step is an important parameter that requires careful adjustment, while keeping the different time scales of ice and ocean processes in mind. In

190 order to assess the coupling frequency on the overall performance, two experiments with time steps of 1 and 10 years are compared. The experiments have a total number of 200 and 20 coupling iterations, respectively, and the individual coupled model simulations start from quasi-equilibrium conditions.

The total runtime required for 200 years model time is $22\,700\,\text{s}$ and $13\,700\,\text{s}$ with a coupling time step of 1 and 10 years, respectively. Figure 8 shows the runtime required for each of the individual components within the coupling framework. With

195 a 10 year coupling time step, the core runtime of MOM5 (90%) including necessary postprocessing (2%) requires the biggest share of total runtime in the coupled setup. The PISM runtime (5%) as well as the time needed for the coupling preprocessing (<1%) and intermodel processing (<2%) routines are almost negligible. This means that in the given setup, coupling the ice sheet model PISM to the ocean model MOM5, comes with minimal overhead compared to standalone ocean simulations, when using a coupling time step of 10 years.

200 In the experiment using a yearly coupling time step, total MOM5 execution times increase slightly ($13\,280\,\text{s}$) compared to 10 yearly coupling ($12\,330\,\text{s}$). The ocean model postprocessing (9%) and intermodel processing routines (6%) are taking a bigger share of the total runtime as they are invoked 10 times as often as in the decennial coupling configuration. PISM runtimes are about 7 times greater for yearly coupling (20% of total runtime), although the total model integration period in PISM is the same in both experiments. This is due to the model initialisation as well as reading and writing of input/output files dominating

205 the PISM execution of 1 model year, which is reasonable as PISM is designed, and usually used, for much longer integration times. Overall, the total execution time increases by about 65% in the yearly coupled setup compared to the run with a coupling time step of 10 years.

5.2 Energy and mass conservation

210 In a coupled model, conservation of mass and energy is important to ensure that no artificial sources or sinks of these quantities are introduced through the coupling mechanism. This is especially important in the context of paleo modelling, where simulations can span tens of thousands of years. In the presented ice-ocean coupling framework, prescribed fluxes are applied at the open system boundaries, e.g. precipitation from the atmosphere to ice and ocean or river runoff from land to ocean. To check that the total amount of mass and energy stocks is constant in the coupled system over the model integration, we assess virtual

215 quantities. Those are obtained by subtracting the applied surface fluxes from the total mass and energy stocks calculated in the
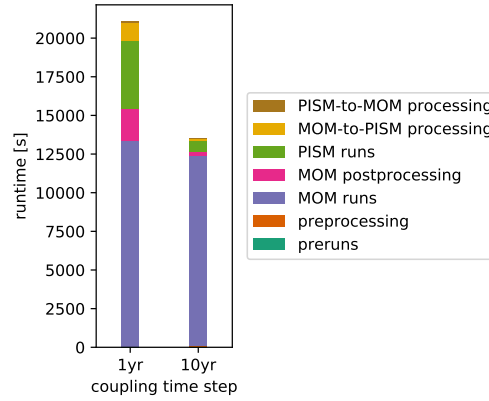
Geoscientific
Model Development
Discussions

Figure 8. Runtimes of coupled PISM-MOM5 setup for 200 years model time, using 32 cores and coupling time steps of 1 and 10 years. PISM runtimes include PICO and MOM5 runtimes include SIS and FMS components. The elapsed time for individual components of the coupling framework is aggregated and stacked in the same order as in the legend. The time required for *preruns*, *preprocessing* and *PISM-to-MOM processing* are small compared to the other components and thus almost not or not perceptible in the Figure.

model (see Eq. (1) for mass). If the virtual model mass across the model domains m_v is constant with fluctuations in the order of machine precision, as denoted in Eq. (2), conservation of mass is achieved.

$$m_\mathrm{v} = (m_\mathrm{o} + m_\mathrm{si} - smb_\mathrm{osi} - d_\mathrm{osi}) + (m_\mathrm{li} - smb_\mathrm{li}) \tag{1}$$

$$\frac{d}{dt}m_\mathrm{v} \sim 0\,\mathrm{Gt/a} \tag{2}$$

220   The masses of the ocean, sea ice and land ice models are represented by $m_\mathrm{o}, m_\mathrm{si}$ and m_li respectively, while smb_osi and smb_li denote the surface mass balance of the ocean-sea ice model MOM5/SIS and the land ice model PISM, respectively. The internal model drift of mass in MOM5/SIS is described by d_osi ($\approx 4 \cdot 10^{15}\,\mathrm{kg}$ in 200 years) and needs to be considered in the computation of virtual model mass in Eq. (1). The absolute and relative mass conservation errors are calculated according to Eq. (3) and (4), respectively.

225    $$e_\mathrm{abs}^\mathrm{m} = m_\mathrm{v} - \overline{m_\mathrm{v}} \tag{3}$$

$$e_\mathrm{rel}^\mathrm{m} = e_\mathrm{abs}^\mathrm{m}/\overline{m_\mathrm{v}} \tag{4}$$

The relative mass conservation error $e_\mathrm{rel}^\mathrm{m}$ (see Eq. (4)) is shown in Fig. 9a for 200 model years with a yearly coupling time step. Regarding the order of magnitude of land ice mass $\mathcal{O}(m_\mathrm{li}) = 10^{19}\,\mathrm{kg}$ which is given in single precision (≈ 7 decimal digits) output format and the order of magnitude of ocean and sea ice mass $\mathcal{O}(m_\mathrm{o} + m_\mathrm{si}) = 10^{21}\,\mathrm{kg}$, given in double precision
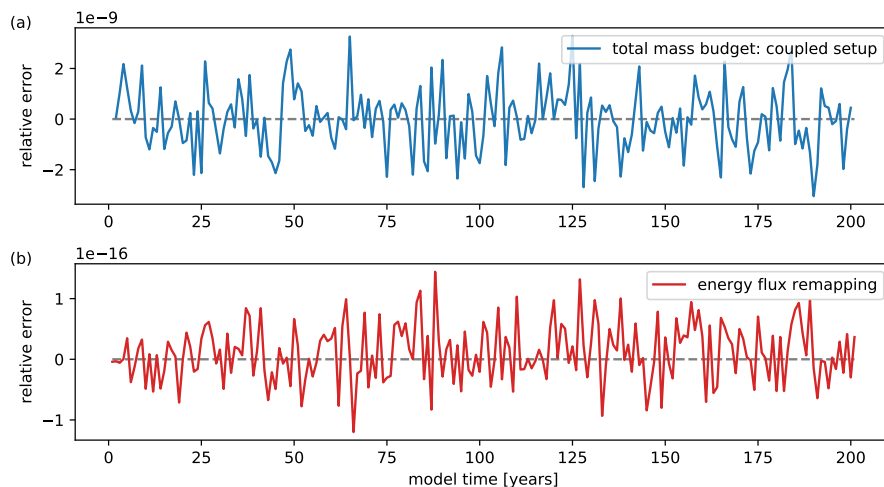
Figure 9. Relative error of virtual mass progression in the coupled ice-ocean system which excludes mass changes applied through surface fluxes and the MOM5/SIS internal model drift (a). Relative error through remapping energy flux from PISM to MOM5 grid (b).

(≈ 16 decimal digits) format, the shown fluctuations in the order of 10^{-9} are reasonable. As the relative mass error does not show a trend, no systematic error is introduced through the coupling procedure.

As PISM does not provide diagnostic variables to record incoming and outgoing energy fluxes across its model boundaries, an analysis of the total amount of enthalpy in the coupled ice-ocean system could not be easily derived. However it is possible to show that no systematic error is induced during remapping the energy flux from PISM to MOM5 grid. Figure 9b shows the relative energy flux remapping error of the test run undertaken in Section 5.1, which is in the order of double machine precision $\mathcal{O}(1e^{-16})$.

6 Discussion

The framework presented here to couple the ice model PISM to the ocean model MOM5 via PICO fulfills all three goals stated in the Introduction, which are (1) mass and energy conservation across both model domains, (2) an efficient as well as (3) generic and flexible coupling framework design:

As described in Section 5.2, mass conservation across both model domains can be assured. Furthermore, the remapping scheme for energy fluxes is conservative as well. Compared to the required run time of MOM5, the framework routines are very efficient when choosing a reasonable coupling time step of 10 years. More frequent coupling causes a larger overhead, as reading and writing the complete model state of PISM to and from files is relatively expensive for very short simulation times. The third criterion is fulfilled by the chosen offline coupling approach, which provides a generic and flexible design by making use of the model-related flexibility concerning grid resolution and degree of parallelisation. This does not easily apply to the alternative approach of online coupling, which will be discussed below.

The chosen offline coupling framework executes the two different models alternately and independently and takes care about redistributing the input and output files across the models as explained in Section 3. However, it is also conceivable to adopt an

250 online coupling approach, where the ice and ocean model code are consolidated into one code structure (Galton-Fenzi et al., 2020). Consequently, the exchange of variables of both models can take place through access to the same shared memory instead of writing the required variables to disk and reading from there again, as it is done in offline coupling. The downside is that a potential integration of PISM into the existing code structure of the ocean model MOM5 and its driver would require heavy modifications and modularisation of the PISM main routine which is responsible for model initialisation, the time step-

255 ping routines, disk I/O, stock checking, etc. Similarly the ocean model main routine would have to be extended to integrate all relevant PISM parts at the right place including MPI parallel mechanisms for data exchange between the submodels. Synchro- nisation of the PISM adaptive time step and the fixed ocean model time step would be a further issue, also keeping in mind that the comparably small ocean time step of a few hours is not applicable for the ice model: PISM can have a time step of around 0.5 years close to equilibrium with $16\,\mathrm{km}$ resolution due to the longer characteristic timescales of ice dynamics. The

260 fact that both models are written in different programming languages (C++ and Fortran) imposes its own barriers. A possible benefit of the described online coupling is less disk I/O overhead, which is especially present for small coupling time steps in the offline coupling approach (see Sec. 5.1). However, that does not outweigh the high initial and ongoing development effort which arises through writing and maintaining modified versions from the main model versions. Offline coupling comes with the advantage, that only very minimal modifications of the existing models' source code are necessary. This makes it fairly

265 easy to even replace the ice or ocean model in use with similar existing models, like using MOM5's successor MOM6. A further benefit of the offline coupling approach is, that it allows easily to run several independent instances of PISM, e.g. for Antarctica and Greenland, at the same time.

Furthermore, the coupling implementation exhibits certain simplifications that can be subject of future improvements. As

270 described in Section 4.2, the mass and energy fluxes computed from PISM output are given as input to the ocean surface rather than being distributed throughout the water column - a limitation of MOM5. A more realistic input depth into the ocean would be the lower edge of the ice shelf front (see start of upper green arrow in Fig. 3; Garabato et al., 2017) which could be determined as the average ice-shelf depth of the last PICO box . However, considering the turbulence in the ocean mixed layer, the simplification of surface input seems reasonable for most cases.

275 Mass and energy fluxes are composed of basal melting, surface runoff and calving and provided as input to the southernmost ocean cells (see Sec. 4.2). Icebergs can however travel substantial distances before they have been melted completely and thus continuously distribute mass and energy fluxes into the ocean (Tournadre et al., 2016). The resulting spatial distribution of iceberg fluxes can introduce biases in sea-ice formation, ocean temperatures, and salinities around Antarctica (Stern et al., 2016). Currently this not considered in our framework and may be simulated by an additional iceberg model (like described in

280 Martin and Adcroft, 2010) in the future.

Another simplification is contained in the energy flux description from ice to ocean. As explained in Section 4.2, the flux is calculated as the energy transferred through phase change from frozen ice to liquid water. Diffusion of heat through the ice and

energy required to warm up melt water to ambient ocean temperatures are currently not considered as they are estimated to be comparably small (Holland and Jenkins, 1999).

285 During long simulations where glacial and interglacial periods are alternating, large amounts of water are transferred between oceans and ice sheets. Through significant changes in the sea level, whole ocean cells can be subject to wetting or drying. The land-ocean mask needs to be adapted accordingly during the simulation including a meaningful way to handle mass and energy stocks. The current framework is not capable of managing such changes yet, but development is currently in progress.

In the coupling framework, ocean input for PICO is averaged over the entire basin, not taking into account horizontal differ-290 ences such as cavity in- and outflow regions and possible modifications of water masses on the continental shelf. Furthermore, complex processes determine what water masses make their way from the open ocean onto the continental shelf and to the grounding lines (Nakayama et al., 2018; Wåhlin et al., 2020). However, in our coarse grid setup of MOM5, bathymetry and circulation on the continental shelf are only partly represented (see also Fig. 1b). PICO currently does not represent circulation patterns besides the vertical overturning circulation, and they hence need to be considered in the tuning process of the PICO 295 parameters.

In this study we focus on the technical implementation of the coupling framework. A re-evaluation of ocean model performance at intermediate depths around the Antarctic margin is required for physically meaningful simulations of the coupled ocean-ice sheet system. The difficulties to accurately simulate Antarctic shelf dynamics and deep water formation in the Southern Ocean with ocean general circulation models is a long standing issue for the ocean modelling community, with almost no 300 models of the CMIP5 generation able to do this successfully (Heuzé et al., 2013). MOM5 is no exception, and exhibits large positive temperature biases in the top 1000 m of the water column, in many cases causing the temperature to rise above freezing and induce unrealistic melting of ice shelves. The improvement of these biases is the subject of ongoing work via the implementation and tuning of the new MOM6 ocean model. An approach to deal with remaining temperature biases could be using ocean model anomalies that are added to observed fields as in ISMIP6 (Jourdain et al., in review, 2019; Nowicki et al., in 305 review, 2020) or regional temperature corrections as used in Lazeroms et al. (2018) and Jourdain et al. (in review, 2019) that are estimated during the tuning process of PICO. While appropriate for present-day simulations, for which we have observations, it is as yet unclear how these biases might be addressed for transient simulations on multi-millennial time-scales. These open issues, including the choice of the coupling time step under physical aspects, will be considered in a future study.

310 Overall, despite the limitations discussed above, the coarse grid setup of MOM5 in combination with the representation of the ice pump mechanism in PICO, makes large-scale and long-term ice-ocean coupling possible at an appropriate level of complexity.

7 Conclusions

In this study we focus on the technical approach and conservation aspects of coupling a large-scale configuration of the ice 315 sheet model PISM and a coarse grid resolution setup of the ocean model MOM5 via the cavity module PICO. This allows to

Geoscientific
Model Development
Discussions

capture the typical overturning circulation in ice-shelf cavities that cannot be modeled in large-scale ocean models. We can assure that conservation of mass and energy is obtained in the coupled system while having a computationally efficient and flexible coupling setup. Using this framework, which is openly available and can also be transferred to other ice-sheet and ocean general circulation models, feedbacks between the ice and ocean can be analysed in large-scale or long-term modelling

320   studies. In future work, the physical processes and feedbacks between ice-sheet, ice shelves and ocean will be further analyzed and the interaction strengths can be evaluated on various timescales, from decades to multi-millennial simulations.

Code and data availability.   The coupling framework code is hosted at https://github.com/m-kreuzer/PISM-MOM_coupling (last accessed: August 24, 2020). The exact version used in this paper has been tagged in the repository as v1.0.2 and is archived via Zenodo (https://doi.org/10.5281/zenodo.3998126, last accessed: August 24, 2020). The code makes use of the software tools Climate Data Operator (CDO,

325   version 1.9.6, Schulzweida (2019); https://doi.org/10.5281/zenodo.3991595, last accessed: August 24, 2020) as well as the netCDF Operator (NCO, version 4.7.8, Zender (2018); https://doi.org/10.5281/zenodo.1490166, last accessed: August 24, 2020). The Parallel Ice Sheet Model (PISM) was used in version 1.1.1 (https://doi.org/10.5281/zenodo.3990026, last accessed: August 24, 2020) and the Modular Ocean Model (MOM) was used in version 5.1.0 with slight modifications as archived in https://doi.org/10.5281/zenodo.3991665 (last accessed: August 24, 2020). All data used in the tests above is archived in https://doi.org/10.5281/zenodo.3997778 (last accessed: August 24, 2020).

330   *Author contributions.*   MK wrote and implemented the coupling framework and performed the analysis. RW, GF and SP conceived the study. MK and RR designed the coupling strategy via PICO. SP and WH provided support with the setup and use of MOM5. RR and TA provided support with the use of PISM. RR contributed to shaping the manuscript. MK prepared the manuscript with input and feedback from all co-authors.

Competing interests.   The authors declare that they have no conflict of interest.

References

350   Albrecht, T., Winkelmann, R., and Levermann, A.: Glacial-cycle simulations of the Antarctic Ice Sheet with the Parallel Ice Sheet Model (PISM) – Part 1: Boundary conditions and climatic forcing, The Cryosphere, 14, 599–632, https://doi.org/10.5194/tc-14-599-2020, 2020.

Asay-Davis, X. S., Cornford, S. L., Durand, G., Galton-Fenzi, B. K., Gladstone, R. M., Gudmundsson, G. H., Hattermann, T., Holland, D. M., Holland, D., Holland, P. R., Martin, D. F., Mathiot, P., Pattyn, F., and Seroussi, H.: Experimental design for three interrelated marine ice sheet and ocean model intercomparison projects: MISMIP v. 3 (MISMIPt), ISOMIP v. 2 (ISOMIP+) and MISOMIP v. 1 (MISOMIP1),

355   Geoscientific Model Development, 9, 2471–2497, https://doi.org/10.5194/gmd-9-2471-2016, 2016.

Asay-Davis, X. S., Jourdain, N. C., and Nakayama, Y.: Developments in Simulating and Parameterizing Interactions Between the Southern Ocean and the Antarctic Ice Sheet, Current Climate Change Reports, 3, 316–329, https://doi.org/10.1007/s40641-017-0071-0, 2017.

Bronselaer, B., Winton, M., Griffies, S. M., Hurlin, W. J., Rodgers, K. B., Sergienko, O. V., Stouffer, R. J., and Russell, J. L.: Change in future climate due to Antarctic meltwater, Nature, 564, 53–58, https://doi.org/10.1038/s41586-018-0712-z, 2018.

360   Bueler, E. and Brown, J.: Shallow shelf approximation as a "sliding law" in a thermomechanically coupled ice sheet model, Journal of Geophysical Research: Earth Surface, 114, https://doi.org/10.1029/2008JF001179, 2009.

Bueler, E., Brown, J., and Lingle, C.: Exact solutions to the thermomechanically coupled shallow-ice approximation: effective tools for verification, Journal of Glaciology, 53, 499–516, https://doi.org/10.3189/002214307783258396, 2007.

Depoorter, M. A., Bamber, J. L., Griggs, J. A., Lenaerts, J. T. M., Ligtenberg, S. R. M., van den Broeke, M. R., and Moholdt, G.: Calving

365   fluxes and basal melt rates of Antarctic ice shelves, Nature, 502, 89–92, https://doi.org/10.1038/nature12567, 2013.

De Rydt, J. and Gudmundsson, G. H.: Coupled ice shelf-ocean modeling and complex grounding line retreat from a seabed ridge, Journal of Geophysical Research: Earth Surface, 121, 865–880, https://doi.org/10.1002/2015JF003791, 2016.

Dinniman, M., , Asay-Davis, X., Galton-Fenzi, B., Holland, P., Jenkins, A., and Timmermann, R.: Modeling Ice Shelf/Ocean Interaction in Antarctica: A Review, Oceanography, 29, 144–153, https://doi.org/10.5670/oceanog.2016.106, 2016.

370   Donat-Magnin, M., Jourdain, N. C., Spence, P., Le Sommer, J., Gallée, H., and Durand, G.: Ice-Shelf Melt Response to Changing Winds and Glacier Dynamics in the Amundsen Sea Sector, Antarctica, Journal of Geophysical Research: Oceans, 122, 10 206–10 224, https://doi.org/10.1002/2017JC013059, 2017.

Favier, L., Jourdain, N. C., Jenkins, A., Merino, N., Durand, G., Gagliardini, O., Gillet-Chaulet, F., and Mathiot, P.: Assessment of sub-shelf melting parameterisations using the ocean–ice-sheet coupled model NEMO(v3.6)–Elmer/Ice(v8.3), Geoscientific Model Development,

375   12, 2255–2283, https://doi.org/10.5194/gmd-12-2255-2019, 2019.

Fürst, J. J., Durand, G., Gillet-Chaulet, F., Tavard, L., Rankl, M., Braun, M., and Gagliardini, O.: The safety band of Antarctic ice shelves, Nature Climate Change, 6, 479–482, https://doi.org/10.1038/nclimate2912, 2016.

Galbraith, E. D., Kwon, E. Y., Gnanadesikan, A., Rodgers, K. B., Griffies, S. M., Bianchi, D., Sarmiento, J. L., Dunne, J. P., Simeon, J., Slater, R. D., Wittenberg, A. T., and Held, I. M.: Climate Variability and Radiocarbon in the CM2Mc Earth System Model, Journal of

380   Climate, 24, 4230–4254, https://doi.org/10.1175/2011JCLI3919.1, 2011.

Galton-Fenzi, B., Gladstone, R., Zhao, C., Gwyther, D., Moore, J., and Zwinger, T.: Progress towards coupling ice sheet and ocean models, EGU General Assembly 2020, Online, 4-8 May 2020, EGU2020-11738, https://doi.org/10.5194/egusphere-egu2020-11738, 2020.

Ganopolski, A. and Brovkin, V.: Simulation of climate, ice sheets and CO_2 evolution during the last four glacial cycles with an Earth system model of intermediate complexity, Climate of the Past, 13, 1695–1716, https://doi.org/10.5194/cp-13-1695-2017, 2017.

385   Garabato, A. C. N., Forryan, A., Dutrieux, P., Brannigan, L., Biddle, L. C., Heywood, K. J., Jenkins, A., Firing, Y. L., and Kimura, S.: Vigor-
ous lateral export of the meltwater outflow from beneath an Antarctic ice shelf, Nature, 542, 219–222, https://doi.org/10.1038/nature20825,
2017.

Gierz, P., Lohmann, G., and Wei, W.: Response of Atlantic overturning to future warming in a coupled atmosphere-ocean-ice sheet model,
Geophysical Research Letters, 42, 6811–6818, https://doi.org/10.1002/2015gl065276, 2015.

390   Goelzer, H., Huybrechts, P., Loutre, M.-F., and Fichefet, T.: Last Interglacial climate and sea-level evolution from a coupled ice sheet–climate
model, Climate of the Past, 12, 2195–2213, https://doi.org/10.5194/cp-12-2195-2016, 2016.

Golledge, N., Keller, E., Gomez, N., Naughten, K., Bernales, J., Trusel, L., and Edwards, T.: Global environmental consequences of twenty-
first-century ice-sheet melt, Nature, 566, 65–72, https://doi.org/10.1038/s41586-019-0889-9, 2019.

Griffies, S. M.: Elements of the Modular Ocean Model (MOM), Tech. Rep. GFDL Ocean Group Technical Report No. 7, NOAA/Geophysical
395   Fluid Dynamics Laboratory, https://mom-ocean.github.io/assets/pdfs/MOM5_manual.pdf, 2012.

Gudmundsson, G. H., Paolo, F. S., Adusumilli, S., and Fricker, H. A.: Instantaneous Antarctic ice sheet mass loss driven by thinning ice
shelves, Geophysical Research Letters, 46, 13 903–13 909, https://doi.org/10.1029/2019gl085027, 2019.

Hellmer, H. H., Kauker, F., Timmermann, R., and Hattermann, T.: The Fate of the Southern Weddell Sea Continental Shelf in a Warming
Climate, Journal of Climate, 30, 4337–4350, https://doi.org/10.1175/JCLI-D-16-0420.1, 2017.

400   Heuzé, C., Heywood, K. J., Stevens, D. P., and Ridley, J. K.: Southern Ocean bottom water characteristics in CMIP5 models, Geophysical
Research Letters, 40, 1409–1414, https://doi.org/10.1002/grl.50287, 2013.

Hillenbrand, C.-D., Smith, J. A., Hodell, D. A., Greaves, M., Poole, C. R., Kender, S., Williams, M., Andersen, T. J., Jernas, P. E., Elderfield,
H., Klages, J. P., Roberts, S. J., Gohl, K., Larter, R. D., and Kuhn, G.: West Antarctic Ice Sheet retreat driven by Holocene warm water
incursions, Nature, 547, 43–48, https://doi.org/10.1038/nature22995, 2017.

405   Holland, D. M. and Jenkins, A.: Modeling Thermodynamic Ice–Ocean Interactions at the Base of an Ice Shelf, Journal of Physical Oceanog-
raphy, 29, 1787–1800, https://doi.org/10.1175/1520-0485(1999)029<1787:mtioia>2.0.co;2, 1999.

Holland, P. R., Bracegirdle, T. J., Dutrieux, P., Jenkins, A., and Steig, E. J.: West Antarctic ice loss influenced by internal climate variability
and anthropogenic forcing, Nature Geoscience, 12, 718–724, https://doi.org/10.1038/s41561-019-0420-9, 2019.

Jenkins, A., Shoosmith, D., Dutrieux, P., Jacobs, S., Kim, T. W., Lee, S. H., Ha, H. K., and Stammerjohn, S.: West Antarctic Ice Sheet retreat
410   in the Amundsen Sea driven by decadal oceanic variability, Nature Geoscience, 11, 733–738, https://doi.org/10.1038/s41561-018-0207-4,
2018.

Jourdain, N. C., Asay-Davis, X., Hattermann, T., Straneo, F., Seroussi, H., Little, C. M., and Nowicki, S.: A protocol for calculating basal
melt rates in the ISMIP6 Antarctic ice sheet projections, The Cryosphere Discussions, https://doi.org/10.5194/tc-2019-277, in review,
2019.

415   Kageyama, M., Harrison, S. P., Kapsch, M.-L., Löfverström, M., Lora, J. M., Mikolajewicz, U., Sherriff-Tadano, S., Vadsaria, T., Abe-Ouchi,
A., Bouttes, N., Chandan, D., LeGrande, A. N., Lhardy, F., Lohmann, G., Morozova, P. A., Ohgaito, R., Peltier, W. R., Quiquet, A., Roche,
D. M., Shi, X., Schmittner, A., Tierney, J. E., and Volodin, E.: The PMIP4-CMIP6 Last Glacial Maximum experiments: preliminary results
and comparison with the PMIP3-CMIP5 simulations, Climate of the Past, https://doi.org/10.5194/cp-2019-169, in review, 2020.

Lazeroms, W. M. J., Jenkins, A., Gudmundsson, G. H., and van de Wal, R. S. W.: Modelling present-day basal melt rates for Antarctic ice
420   shelves using a parametrization of buoyant meltwater plumes, The Cryosphere, 12, 49–70, https://doi.org/10.5194/tc-12-49-2018, 2018.

Levermann, A., Winkelmann, R., Nowicki, S., Fastook, J. L., Frieler, K., Greve, R., Hellmer, H. H., Martin, M. A., Meinshausen, M., Mengel, M., Payne, A. J., Pollard, D., Sato, T., Timmermann, R., Wang, W. L., and Bindschadler, R. A.: Projecting Antarctic ice discharge using response functions from SeaRISE ice-sheet models, Earth System Dynamics, 5, 271–293, https://doi.org/10.5194/esd-5-271-2014, 2014.

Levermann, A., Winkelmann, R., Albrecht, T., Goelzer, H., Golledge, N. R., Greve, R., Huybrechts, P., Jordan, J., Leguy, G., Martin, D.,
425 Morlighem, M., Pattyn, F., Pollard, D., Quiquet, A., Rodehacke, C., Seroussi, H., Sutter, J., Zhang, T., Breedam, J. V., Calov, R., DeConto, R., Dumas, C., Garbe, J., Gudmundsson, G. H., Hoffman, M. J., Humbert, A., Kleiner, T., Lipscomb, W. H., Meinshausen, M., Ng, E., Nowicki, S. M. J., Perego, M., Price, S. F., Saito, F., Schlegel, N.-J., Sun, S., and van de Wal, R. S. W.: Projecting Antarctica's contribution to future sea level rise from basal ice shelf melt using linear response functions of 16 ice sheet models (LARMIP-2), Earth System Dynamics, 11, 35–76, https://doi.org/10.5194/esd-11-35-2020, 2020.

430 Lewis, E. L. and Perkin, R. G.: Ice pumps and their rates, Journal of Geophysical Research: Oceans, 91, 11 756–11 762, https://doi.org/10.1029/JC091iC10p11756, 1986.

Lowry, D. P., Golledge, N. R., Bertler, N. A. N., Jones, R. S., and McKay, R.: Deglacial grounding-line retreat in the Ross Embayment, Antarctica, controlled by ocean and atmosphere forcing, Science Advances, 5, eaav8754, https://doi.org/10.1126/sciadv.aav8754, 2019.

Martin, T. and Adcroft, A.: Parameterizing the fresh-water flux from land ice to ocean with interactive icebergs in a coupled climate model,
435 Ocean Modelling, 34, 111–124, https://doi.org/10.1016/j.ocemod.2010.05.001, 2010.

Nakayama, Y., Menemenlis, D., Zhang, H., Schodlok, M., and Rignot, E.: Origin of Circumpolar Deep Water intruding onto the Amundsen and Bellingshausen Sea continental shelves, Nature Communications, 9, https://doi.org/10.1038/s41467-018-05813-1, 2018.

Naughten, K. A., Meissner, K. J., Galton-Fenzi, B. K., England, M. H., Timmermann, R., and Hellmer, H. H.: Future Projections of Antarctic Ice Shelf Melting Based on CMIP5 Scenarios, Journal of Climate, 31, 5243–5261, https://doi.org/10.1175/jcli-d-17-0854.1, 2018.

440 Nowicki, S., Payne, A. J., Goelzer, H., Seroussi, H., Lipscomb, W. H., Abe-Ouchi, A., Agosta, C., Alexander, P., Asay-Davis, X. S., Barthel, A., Bracegirdle, T. J., Cullather, R., Felikson, D., Fettweis, X., Gregory, J., Hatterman, T., Jourdain, N. C., Munneke, P. K., Larour, E., Little, C. M., Morlinghem, M., Nias, I., Shepherd, A., Simon, E., Slater, D., Smith, R., Straneo, F., Trusel, L. D., van den Broeke, M. R., and van de Wal, R.: Experimental protocol for sealevel projections from ISMIP6 standalone ice sheet models, The Cryosphere Discussions, https://doi.org/10.5194/tc-2019-322, in review, 2020.

445 Olbers, D. and Hellmer, H.: A box model of circulation and melting in ice shelf caverns, Ocean Dynamics, 60, 141–153, https://doi.org/10.1007/s10236-009-0252-z, 2010.

Pollard, D., Chang, W., Haran, M., Applegate, P., and DeConto, R.: Large ensemble modeling of the last deglacial retreat of the West Antarctic Ice Sheet: comparison of simple and advanced statistical techniques, Geoscientific Model Development, 9, 1697–1723, https://doi.org/10.5194/gmd-9-1697-2016, 2016.

450 Reese, R., Gudmundsson, G. H., Levermann, A., and Winkelmann, R.: The far reach of ice-shelf thinning in Antarctica, Nature Climate Change, 8, 53–57, https://doi.org/10.1038/s41558-017-0020-x, 2017.

Reese, R., Albrecht, T., Mengel, M., Asay-Davis, X., and Winkelmann, R.: Antarctic sub-shelf melt rates via PICO, The Cryosphere, 12, 1969–1985, https://doi.org/10.5194/tc-12-1969-2018, 2018.

Schulzweida, U.: CDO User Guide (Version 1.9.6), Manual, MPI for Meteorology Hamburg, https://code.mpimet.mpg.de/projects/cdo/
455 embedded/cdo.pdf. Last accessed July 1, 2020, 2019.

Seroussi, H., Nakayama, Y., Larour, E., Menemenlis, D., Morlighem, M., Rignot, E., and Khazendar, A.: Continued retreat of Thwaites Glacier, West Antarctica, controlled by bed topography and ocean circulation, Geophysical Research Letters, 44, 6191–6199, https://doi.org/10.1002/2017GL072910, 2017.

Seroussi, H., Nowicki, S., Payne, A. J., Goelzer, H., Lipscomb, W. H., Abe Ouchi, A., Agosta, C., Albrecht, T., Asay-Davis, X., Barthel, A.,
460   Calov, R., Cullather, R., Dumas, C., Gladstone, R., Golledge, N., Gregory, J. M., Greve, R., Hatterman, T., Hoffman, M. J., Humbert, A.,
     Huybrechts, P., Jourdain, N. C., Kleiner, T., Larour, E., Leguy, G. R., Lowry, D. P., Little, C. M., Morlighem, M., Pattyn, F., Pelle, T., Price,
     S. F., Quiquet, A., Reese, R., Schlegel, N.-J., Shepherd, A., Simon, E., Smith, R. S., Straneo, F., Sun, S., Trusel, L. D., Van Breedam, J.,
     van de Wal, R. S. W., Winkelmann, R., Zhao, C., Zhang, T., and Zwinger, T.: ISMIP6 Antarctica: a multi-model ensemble of the Antarctic
     ice sheet evolution over the 21st century, The Cryosphere Discussions, https://doi.org/10.5194/tc-2019-324, in review, 2020.

465 Shepherd, A., Ivins, E., Rignot, E., Smith, B., Van den Broeke, M., Whitehouse, P., Briggs, K., Joughin, I., Krinner, G., Nowicki, S., Payne,
     A., Scambos, T., Schlegel, N., Aa, G., Agosta, C., Ahlstrøm, A., Babonis, G., Barletta, V., Blazquez, A., and Wouters, B.: Mass balance
     of the Antarctic Ice Sheet from 1992 to 2017, Nature, 558, https://doi.org/10.1038/s41586-018-0179-y, 2018.

Slater, J. A. and Malys, S.: WGS 84 — Past, Present and Future, in: Advances in Positioning and Reference Frames, pp. 1–7, Springer Berlin
     Heidelberg, https://doi.org/10.1007/978-3-662-03714-0_1, 1998.

470 Stern, A. A., Adcroft, A., and Sergienko, O.: The effects of Antarctic iceberg calving-size distribution in a global climate model, Journal of
     Geophysical Research: Oceans, 121, 5773–5788, https://doi.org/10.1002/2016jc011835, 2016.

Sutter, J., Gierz, P., Grosfeld, K., Thoma, M., and Lohmann, G.: Ocean temperature thresholds for Last Interglacial West Antarctic Ice Sheet
     collapse, Geophysical Research Letters, 43, 2675–2682, https://doi.org/10.1002/2016gl067818, 2016.

Taylor, K. E., Stouffer, R. J., and Meehl, G. A.: An Overview of CMIP5 and the Experiment Design, Bulletin of the American Meteorological
475   Society, 93, 485–498, https://doi.org/10.1175/BAMS-D-11-00094.1, 2012.

Timmermann, R. and Goeller, S.: Response to Filchner–Ronne Ice Shelf cavity warming in a coupled ocean–ice sheet model – Part 1: The
     ocean perspective, Ocean Science, 13, 765–776, https://doi.org/10.5194/os-13-765-2017, 2017.

Tournadre, J., Bouhier, N., Girard-Ardhuin, F., and Rémy, F.: Antarctic icebergs distributions 1992–2014, Journal of Geophysical Research:
     Oceans, 121, 327–349, https://doi.org/10.1002/2015jc011178, 2016.

480 Wåhlin, A. K., Steiger, N., Darelius, E., Assmann, K. M., Glessmer, M. S., Ha, H. K., Herraiz-Borreguero, L., Heuzé, C., Jenkins, A., Kim,
     T. W., Mazur, A. K., Sommeria, J., and Viboud, S.: Ice front blocking of ocean heat transport to an Antarctic ice shelf, Nature, 578,
     568–571, https://doi.org/10.1038/s41586-020-2014-5, 2020.

Winkelmann, R., Martin, M. A., Haseloff, M., Albrecht, T., Bueler, E., Khroulev, C., and Levermann, A.: The Potsdam Parallel Ice Sheet
     Model (PISM-PIK) – Part 1: Model description, The Cryosphere, 5, 715–726, https://doi.org/10.5194/tc-5-715-2011, 2011.

485 Winton, M.: A Reformulated Three-Layer Sea Ice Model, Journal of Atmospheric and Oceanic Technology, 17, 525–531,
     https://doi.org/10.1175/1520-0426(2000)017<0525:ARTLSI>2.0.CO;2, 2000.

Zender, C. S.: netCDF Operator (NCO) User Guide (Version 4.7.8), Manual, http://nco.sf.net/nco.pdf. Last accessed July 1, 2020, 2018.

Ziemen, F. A., Kapsch, M.-L., Klockmann, M., and Mikolajewicz, U.: Heinrich events show two-stage climate response in transient glacial
     simulations, Climate of the Past, 15, 153–168, https://doi.org/10.5194/cp-15-153-2019, 2019.

490 Zwally, H. J., Giovinetto, M. B., Beckley, M. A., and Saba, J. L.: Antarctic and Greenland Drainage Systems, http://icesat4.gsfc.nasa.gov/
     cryo_data/ant_grn_drainage_systems.php. Last accessed July 1, 2020, 2012.